I R A M P
5(1), June 2014, pp. 33-47

ISSN: 2229-3159

Efficient Ultra Short X-ray Laser at 32.8 nm Produced by Optical Field Ionization in Krypton Cluster Jet

E. P. IVANOVA AND A. YU. VINOKHODOV

Institute of Spectroscopy, Russian Academy of Sciences, 142190 Troitsk, Moscow Region, Russian Federation

ABSTRACT: The available experimental measurements of quantum yields of X-ray lasers with λ = 32.8 nm at the $3d^9 4d\ (J=0)$ - $3d^9 4p\ (J=1)$ transition in Kr^{8+} are interpreted. In various experiments, plasma was pumped in gaseous krypton and in krypton cluster jet. Using our model, an original scheme of the X-ray laser with λ = 32.8 nm, implemented in the krypton cluster jet is proposed. An unexpected result is the achievement of quantum yield saturation at a plasma length of ~300 μm at the krypton atom density $n_{Kr} \sim (4\text{-}9)\cdot 10^{19}$ cm^{-3} and electron temperature $T_e \geq 5000$ eV. In this case, the conversion efficiency reaches $\sim 5\cdot 10^{-3}$ of the pump pulse energy. The experimental setup of the highly efficient X-ray laser of subpicosecond duration, implemented in the krypton cluster jet is described in detail.

PACS: 42.55.Vc, 52.38.Ph

Keywords: X-ray lasers, atomic data calculations

I. INTRODUCTION

In the last decade, the interaction of cluster jets with intense infrared laser radiation is studied with the purpose of developing hot dense plasma used as a far ultraviolet source. The mechanism of the formation of such cluster plasma is optical field ionization (OFI) of clusters in jet. One of the directions of such studies is the development of the X-ray laser (XRL) with λ = 1-40 nm. To date, a compact inexpensive XRL in krypton cluster jet with λ = 32.8 nm with a quantum yield of 10^{12} photon/pulse is already created, which is applicable to many types of applications [1]. The conversion efficiency in [1] is $5\cdot 10^{-6}$.

The XRL in the cluster jet is a stage in the way of developing XRLs in solid nanostructured targets, provided sufficient pump laser intensity. An obvious advantage of cluster plasma is relative simplicity of a change in plasma parameters by varying the gas pressure in a back camera connected to a nozzle. High laser intensity implies longitudinal pumping; however, it is accompanied by an increase in radial plasma inhomogeneity as the pump beam passes through the target, which leads to different refractive indices of the propagating beam at various plasma points. Thus, the longer the plasma column, the higher the inhomogeneity along the radius, hence, the larger the divergence of output radiation. The latter leads to coherence loss. To date, it is demonstrated that sufficient coherence at longitudinal pumping is possible in a target of a few millimeters long. In this regard, methods for maintaining coherence by more homogeneous plasma formation due to additional pump pulses are developed. In our opinion, there is the other way, i.e., the search for effective XRLs in plasma of ultrashort length, in which giant gains can be achieved due to a sufficiently high density ($n_i \geq 4\cdot 10^{19}$ cm^{-3}) and temperatures (≥5 keV).

II. FORMULATION OF THE PROBLEM

In [2], three similar XRL schemes based on $^1S_0 - {}^1P_1$ transitions of Ar^{8+}, Kr^{8+}, Xe^{8+} noble gas ions are presented (see Fig. 1 in [2]). For each of indicated ions, a three-level scheme can be implemented due to the strong monopole electron-impact pumping of the upper active level $^1S_0$, rapid radiative emptying of the lower active level $^1P_1$, and the sufficiently strong radiative transition from the upper active level to the lower one. Figure 1 shows simplified laser

schemes where the radiative transition rates determined in this calculation and the wavelengths of the main laser transition are also shown. In [2], the lifetimes of active levels $^1S_0$, $^1P_1$, are given, which allow the conclusions about the probabilities of radiative transitions from these levels.

In Table 1, the transition probabilities for Kr^{8+} calculated by our approach of the relativistic perturbation theory with model potential of zero approximation (RPTMP) are compared to the corresponding data calculated in [2]. The probabilities of radiative transitions from the lower active level to the ground level are in agreement within ~30%. The rates of electron-induced transitions are in satisfactory agreement, while the collision line widths and maximum inversion densities are in excellent agreement. The Doppler width in [2] was calculated at an ion temperature (T_i) close to zero, whereas we use the approximation $T_i = T_e/10$, (T_e is electron temperature). For this reason and also because of the large difference of probability of the radiative transition from the upper active level to the lower one the gain in [2] is approximately five times higher than that determined by the RPTMP value. According to our calculations, the rates of the $^1S_0 - {}^1P_1$ radiative transition are $4.69 \cdot 10^9$, $1.64 \cdot 10^{10}$, and $1.3 \cdot 10^{10}$ s^{-1} for Ar^{8+}, Kr^{8+}, and Xe^{8+}, respectively. These values are significantly lower than the published rates of this transition, which are also in poor agreement with each other. The causes of disagreement in the probabilities of this transition in various theoretical approaches are discussed in [3].

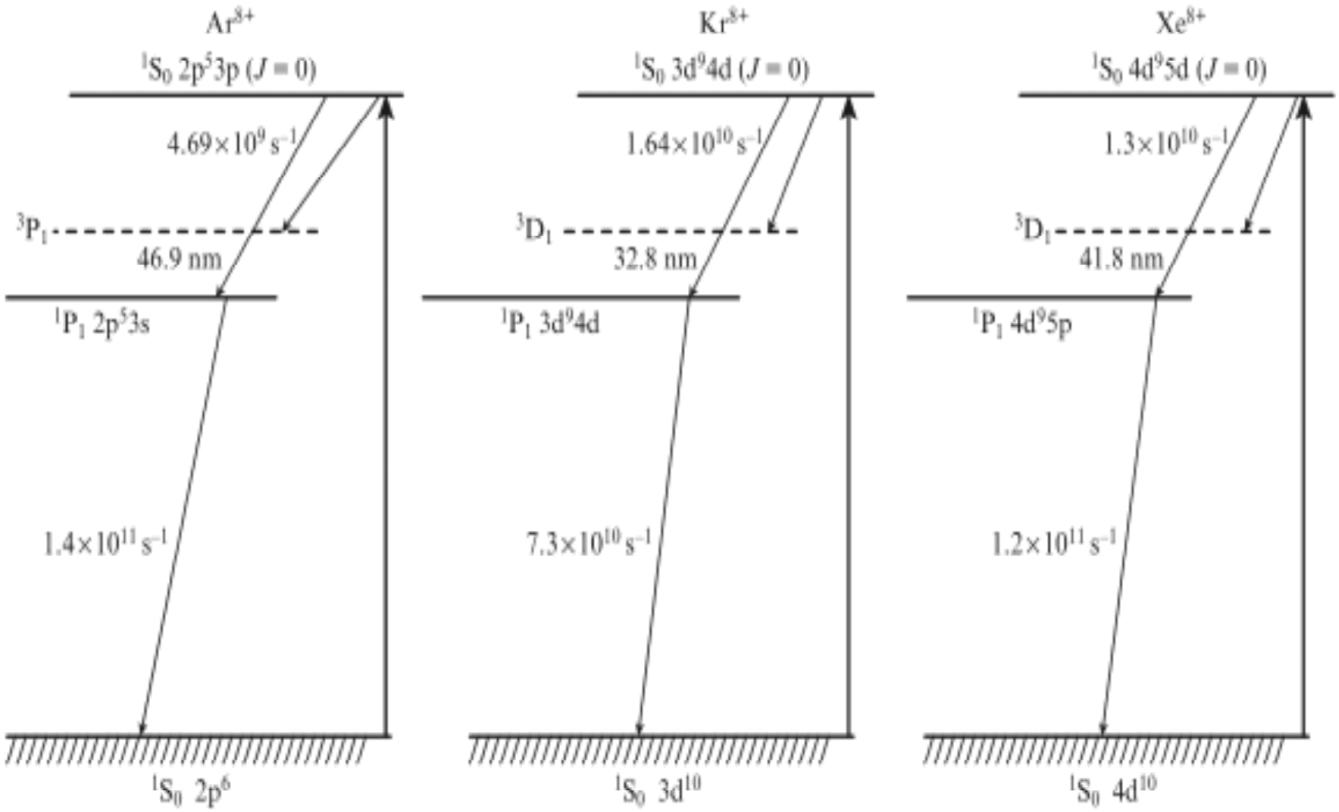

Figure 1: Three schemes of the XRL at the $^1S_0$ - $^1P_1$ transition in Ar^{8+}, Kr^{8+}, and Xe^{8+} noble gas ions

From the upper active level $^1S_0$, a weaker longer-wavelength laser transition to the $^3P_1$ level in Ar^{8+}, as well as $^3D_1$ in Kr^{8+}, Xe^{8+} are also possible; these levels are indicated in Fig. 1 by dashed lines. In Kr^{8+}, the wavelength of this transition is $\lambda_2 \approx 33.5$ nm. The rate of this radiative transition for each ion is approximately three times lower than the rate of the $^1S_0 - {}^1P_1$ lasing transition.

Above-threshold ionization of the atomic system during the interaction with a strong electromagnetic field was justified within the classical theoretical approach in [4]. The threshold electromagnetic field strength for eight-electron ionization in *Ar*, *Kr*, and *Xe* atoms was estimated in [2] using formulas of [4]. For krypton, the threshold intensity was ≥ 10^{17} W/cm^2; ionization of the 9-th electron of the $3d^{10}$ shell in Kr^{8+} requires a nine times higher intensity. Therefore, in [2] and in this paper, we assume that ~90% of ions immediately after exposure to a femtosecond pump pulse are in the Kr^{8+} state. According to [2, 4], the electron energy distribution at the instant of detachment of eight electrons from the krypton atom is eight δ-functions with energies from 12 to 1050 eV. At the Kr^{8+} density of 10^{18} cm^{-3}, electron energy thermalization (maxwellization) occurs in a subpicosecond time interval. This is the time of the order of 100 fs at a density of ≥ 10^{19} cm^{-3}.

For the three indicated ions, Fig. 2 shows the rates of monopole excitation by electron-ion impact from the ground state $^1S_0$ to the upper active states. We note that the data in Fig. 2 are in good agreement with the corresponding results of calculations of other authors. It follows from Fig.2 that the rates of the electron-impact excitation in Ar^{8+} is lower by an order of magnitude than in Kr^{8+} and lower by more ~1.5 orders of magnitude than in Xe^{8+}. Such low pumping rates provide small inversion, so that the maximum gain *g(t)* in Ar^{8+} plasma under optimal conditions do not exceed 1-2 cm^{-1} [5-6]. This is clearly insufficient to obtain a high quantum yield at plasma column lengths of the order of several millimeters.

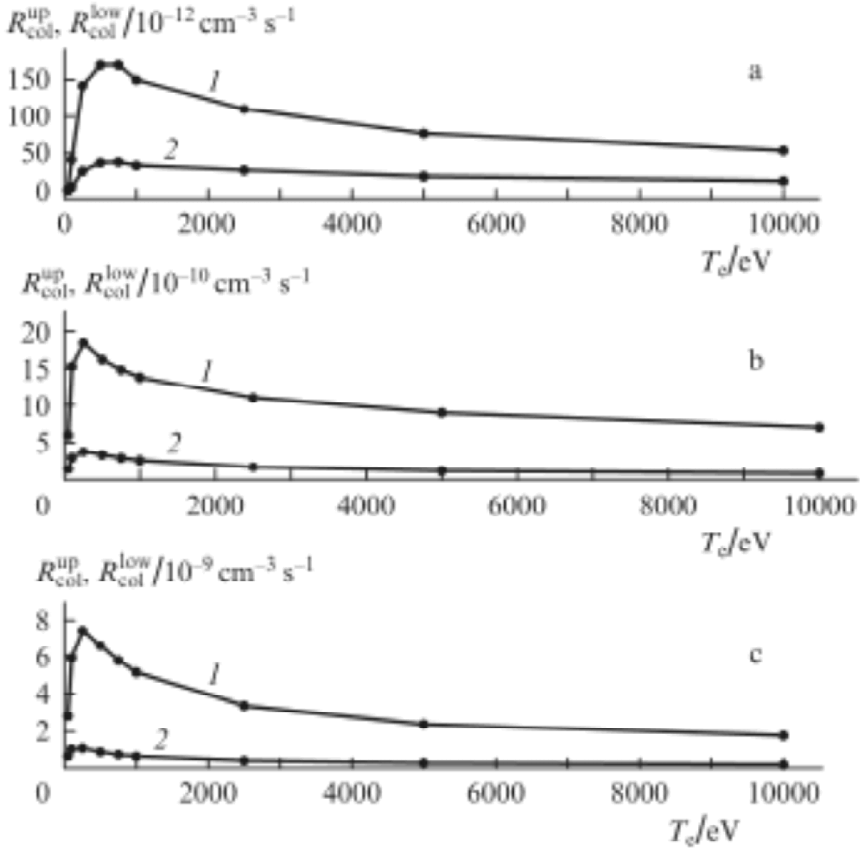

Figure 2: Rates of electron impact excitation of upper [R_{col}^{up}; (1)] and lower [R_{col}^{low}; (2)] working levels in (a) Ar^{8+}, (b) Kr^{8+}, and (c) Xe^{8+} ions.

The model of the efficient XRL with λ = 41.8 nm in *Pd*-like xenon (Xe^{8+}) was developed in [7]. It was assumed that plasma was formed due to the interaction of the xenon cluster jet with the optical field of the femtosecond laser with an intensity of ≥ 10^{16} W/cm^2. In [8], also using the xenon cluster jet, pumping conditions were determined for developing the subpicosecond XRL in Xe^{8+}: the photon quantum yield of 10^{13} photon/pulse is possible from plasma with length L = 0.3 mm and ~20 μm in diameter at the xenon density of $2.5 \cdot 10^{19}$ cm^{-3}.

We can see in Figs. 1 and 2 that the rates of radiative transitions and transitions caused by collisions with electrons in Kr^{8+} are approximately two times lower than in Xe^{8+}. Much the same ratio of rates is also valid for other transitions controlling the kinetics of populations of excited levels in Kr^{8+}. We note that exactly this circumstance causes the unique opportunities for developing the highly efficient XRL of ultrashort duration in Kr^{8+}.

In this study, the atomic-kinetic calculations of the emission spectra of *Ni*- like krypton are performed. In the kinetics of level populations, along with the ground level, 54 excited energy levels of configurations $3d^9 4l$ ($l = 0$-3) and 13 levels of configurations $3p^5 3d^{10} 4s$ and $3p^5 3d^{10} 4p$ below the ionization potential, i.e., a total of 68 levels are taken into account. The consideration of the last 13 highly excited levels is not principal. These levels are taken into account to test the calculation stability over the number of the considered states.

In the calculations, the following assumptions were made.

(i) Plasma is shaped as a cylinder of diameter d and length L as a result of laser beam propagation through a cluster jet of thickness L.

(ii) The pumping pulse parameters are such that plasma with electron temperature T_e, which contains 90% of the ground state Kr^{8+} ion fraction, is formed immediately after the interaction of the laser optical field with clusters.

(iii) The electron (T_e) and ion (T_i) temperatures and plasma diameter (d) are uniform over the volume and unchanged for the lasing time.

(iv) The energy distribution of electrons and ions is assumed to be Maxwellian; the distribution shape plays no substantial role in the calculations of the rates of transitions induced by electron-ion collisions.

(v) The ion temperature in cluster plasma $T_i = T_e$. In plasma formed by the OFI in gaseous krypton, $T_i = T_e/4$.

(vi) We do not calculate the amplification dynamics of spontaneous radiation propagating in plasma. Here one of the possible approaches is the solution of Maxwell-Bloch equations [9-10]. Such calculations are necessary to determine the saturation $g(t)$ along the plasma length L. In the case at hand (as well as in the overwhelming majority of experiments), amplification is observed in the active ion ionization mode in the overionization stages. The active ion lifetime in plasma in principle defines the parameter L. In [11], it is proposed to use the estimate $gL \sim 14$-15 at which saturation along the length is achieved. Here we use a similar approach for determining the saturation length.

(vii) In the calculation, we average the gain $g(t)$ over spatial and temporal coordinates. To this end, we divide the target cylinder into segments smaller than the length of the spatial scale of the pump pulse; then, elementary processes in each segment will occur identically, but with a time delay. In this case, it is sufficient to perform only time averaging for the function $g(t)$. The theoretical model of the calculation is presented in our previous papers [6-8] and references therein.

In section 3, we interpret the results of experimental observations of the spontaneous emission amplification at the transition with $\lambda = 32.8$ nm in Kr^{8+} in plasma formed during the interaction of gaseous krypton with the optical field of the pump laser [12,13-14]. In section 4, we interpret the experimental results [15-16,1] where the active medium was formed during the interaction of the krypton cluster jet with the optical field of the pump laser. The model of the highly efficient XRL of ultrashort duration with $\lambda = 32.8$ nm was calculated in section 5. The experimental setup is discussed in section 6.

III. INTERPRETATION OF THE EXPERIMENTAL RESULTS ON THE X-RAY LASER OBSERVATION IN GASEOUS KRYPTON

The first calculation of the gains $g(t)$ in *Ni*-like krypton (Kr^{8+}) was performed in [12], where the strong dependence of the gains on T_e was noted. The gain was experimentally measured in [13], where plasma in the inverted state was produced by longitudinal laser pumping of gaseous krypton in a cell. The quantum yield of the XRL with $\lambda = 32.8$ nm depending on the cell length was recorded using a CCD camera. Pumping was performed by circularly polarized

radiation of a femtosecond Ti-sapphire laser (760 mJ, 30 fs). Radiation was focused into a point spaced by several millimeters from the input to the cell with krypton. The actual effective diameter was not determined in [13]. According to our calculations, the effective diameter was within $40 \geq d \geq 16$ μm, depending on the plasma density. For comparison with Fig. 5 of [13], Figure 3 shows our theoretical dependences of the quantum yield $N_{out}^{ph}(L)$ of the XRL with $\lambda = 32.8$ nm on the plasma length L. At the known density and geometry, we fitted T_e so that to extremely accurately reproduce the experimental dependence of the quantum yield on L. The value of T_e determined in such a way is 90 eV. This value corresponds to an increase in the quantum yield in the length from 3 mm to 4.5 mm by ~2.5 orders of magnitude. At $L \sim 4$ mm, the experimental curve flattens out in length (see Fig. 5 in [13]), while our model curve in Fig. 3 is still far from flattening. A comparison shows that the pump energy in the experiment was sufficient to only excite plasma with $L \sim 4$ mm. Such an assumption was also made in [13] when discussing the experiment. We note that the second weaker laser line with $\lambda \approx 33.5$ nm was observed in [13]; this transition is shown in Fig. 2 of this work.

To compare the experimental dependence of N_{out}^{ph} on the krypton atomic density n_{Kr} at given T_e and L shown in Fig. 3 in [13], we performed a corresponding calculation at $T_e = 90$ eV and $L = 4.5$ mm. This curve is shown in Fig. 4, its maximum value is normalized to unity. It is significant that the $N_{out}^{ph}(n_{Kr})$ maximum is achieved at the density $n_{Kr} = 20$ Torr if $T_e = 90$ eV; at other T_e, the $N_{out}^{ph}(n_{Kr})$ maximum shifts. Good agreement between our theoretical curve in Fig. 4 and the experimental curve (Fig. 3 of [13]) is achieved, if we take into account the gradual decrease in the active medium diameter from 40 to 16 μm as n_{Kr} changes from 5 to 20 Torr. At $n_{Kr} \geq 20$ Torr, $d \approx 16$ μm. Thus, the value $T_e = 90$ eV was obtained by processing of two independent experiments in [13]. An increase in N_{out}^{ph} by a factor of 200 in the interval of 3-4 mm corresponds to the average $g \sim 24$ cm^{-1}. The time evolution $g(t)$ calculated using the model under consideration is shown in Fig. 5.

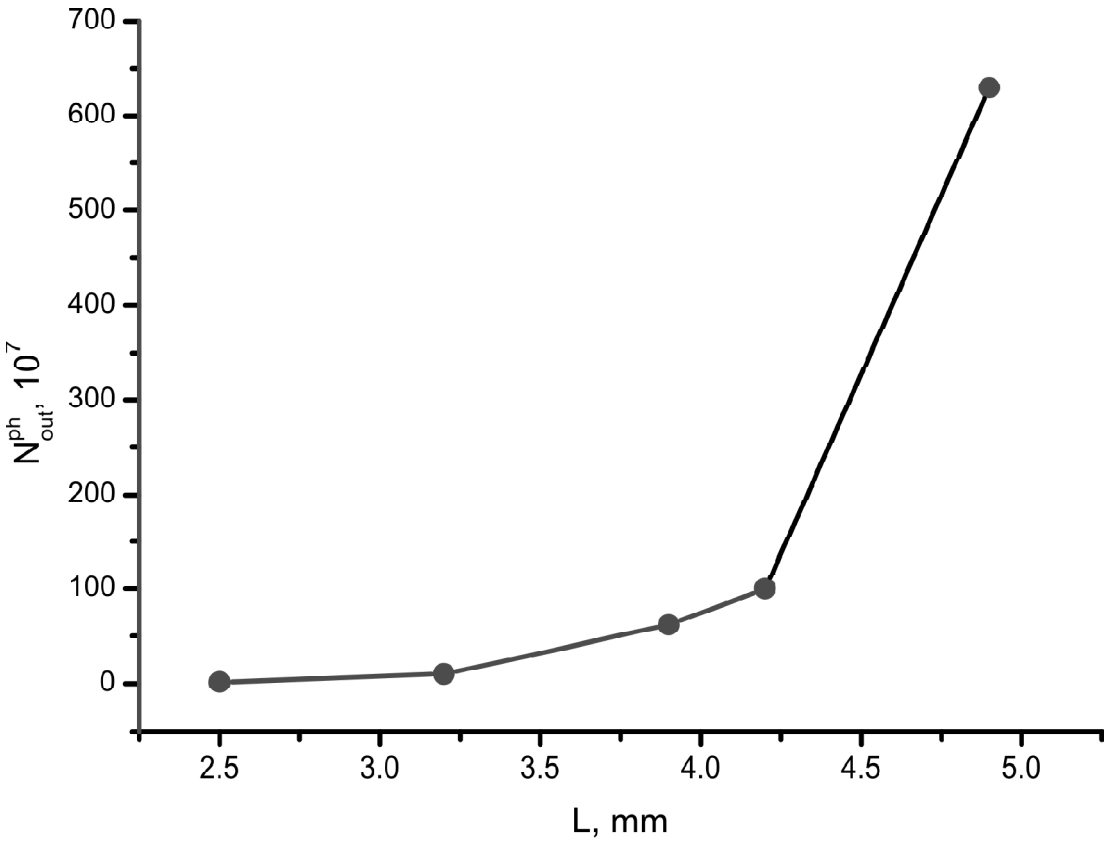

Figure 3: Model calculation of the present study: the dependence of N_{out}^{ph} on the plasma length L, for the comparison with the corresponding experimental data obtained with gaseous krypton plasma [13].

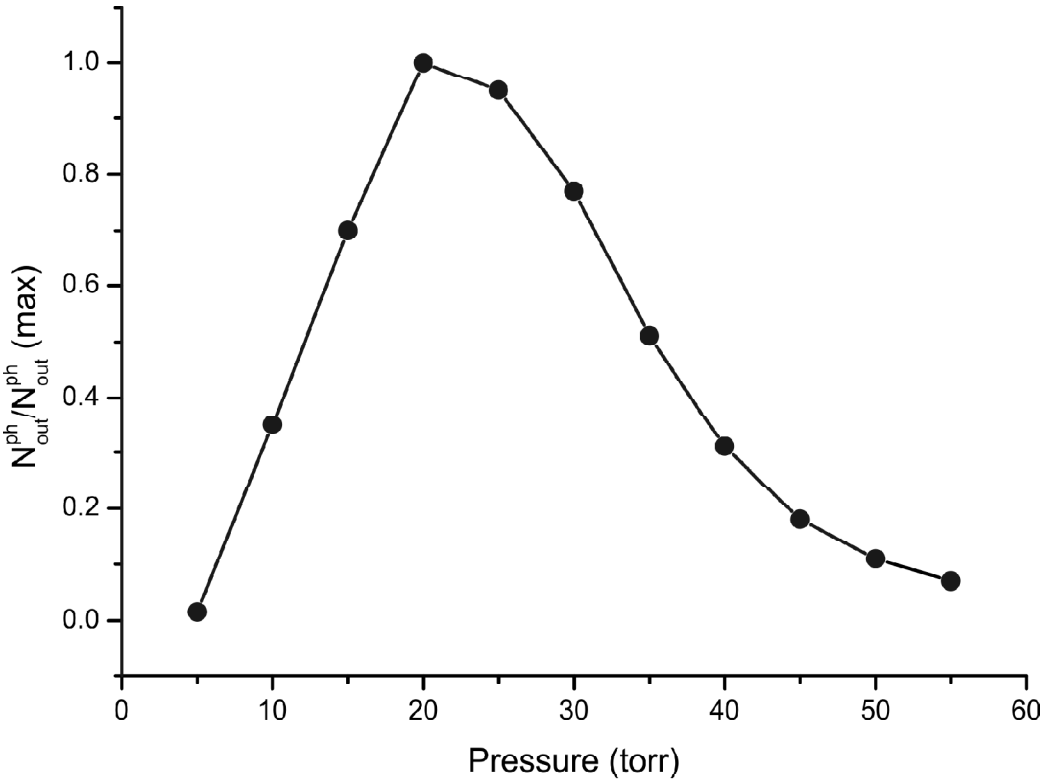

Figure 4: Model calculation of the present study: the dependence of the intensity of the XRL line with λ=32.8 nm in Kr^{8+} on the density, constructed for the comparison with the corresponding experimental data obtained with gaseous plasma [13].

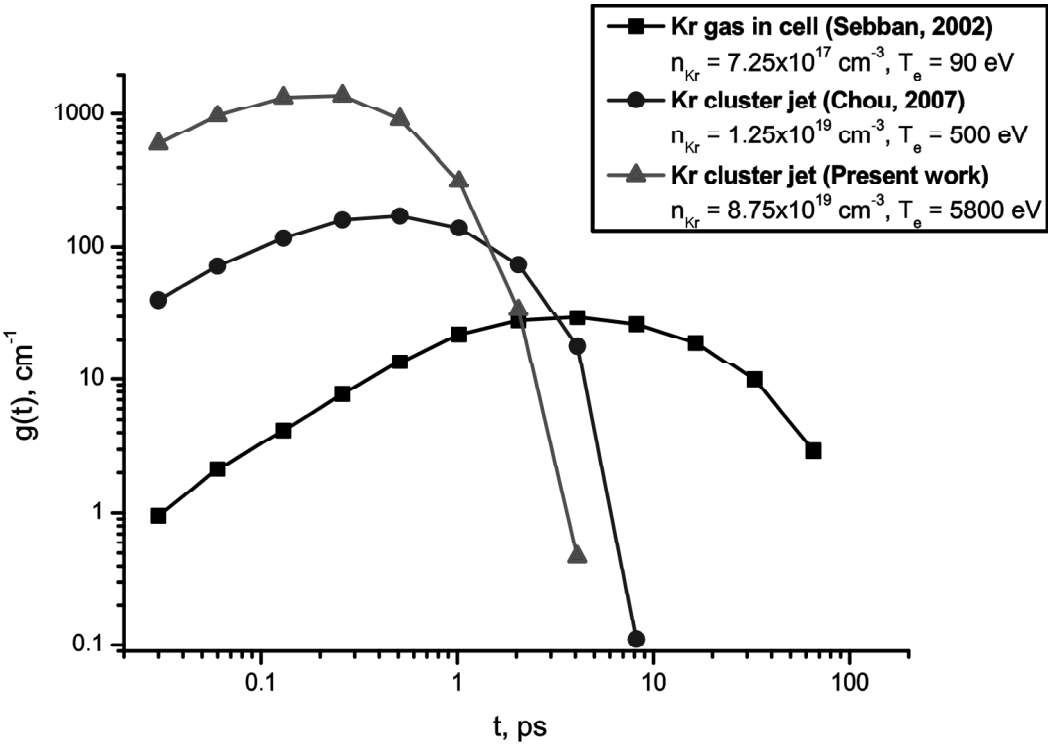

Figure 5: Time evolutions of the gains calculated for the XRL in krypton; squares, circles, and triangles correspond, respectively, to the experiment with gaseous krypton [13], the krypton cluster jet in experiments [15-16], and the model calculation of the present work.

Figure 3 of [13] shows the dependence $N_{out}^{ph}(n_{Xe})$ for a similar experiment in gaseous xenon [14]. This experiment was performed at a significantly lower pump intensity, $I_{pump} = 3 \cdot 10^{16}$ W/cm^2; however, the photon quantum yield at the maximum was higher than in [13] by a factor of 2-3. The value of T_e in the experiment [14] was determined by us as 140 eV. The higher temperature causes a higher quantum yield in [14]. The maximum for xenon in [14] was observed at a gas density of 15 torr. It is not difficult to understand the nature of the extreme dependence of the XRL quantum yield on the density. Let us assume that T_e is fixed; then, pumping, inversion, and N_{out}^{ph} will increase with density. However, as the density increases, level population mixing will be enhanced due to electron-ion collisions; plasma will tend to an equilibrium state, and inversion will decrease. Furthermore, as the density increases, the rate of Kr^{8+} ionization to Kr^{9+}, Kr^{10+}, and higher states will increase due to electron-ion collisions; in this case, the density of active ions/inversion will decrease. The maximum of the N_{out}^{ph} function on the plasma density corresponds to the balance of these processes. As the density further increases, collisional mixing of level populations and Kr^{8+} ionization dominate; in this case, the inversion and N_{out}^{ph} decrease. The position of the N_{out}^{ph} maximum for Kr^{8+} at a higher density than in Xe^{8+} is explained by the fact that level population mixing rates in Kr^{8+} is approximately two times lower than in Xe^{8+}.

We note that the laser line measurement in Xe^{8+} [14] begins at the shortest length $L = 1.5$ mm, whereas the laser line in Kr^{8+} is noticeable only at $L = 3$ mm. This results is explained by the fact that the laser line curve in Kr^{8+} "sinks" in background radiation of plasma at $L < 3$ mm.

Weak amplification of the laser line in Kr^{8+} plasma provides strong evidence for significantly lower T_e resulted from krypton atom OFI, than the theory predicts [4]. According to the calculations of [2] and [13], it follows from formula (3) of [4] that the average electron energy should be ~640 eV after the interaction of the *Kr* atom with circularly polarized light after detachment of eight electrons, which strongly contradicts the experimental value T_e = 90 eV in [13]. The interpretation of the experiments [13-14] shows that atomic electrons with a higher ionization potential (i) require a higher intensity of the optical field and (ii) have a lower kinetic energy after detachment. The statement (i) is obvious; the statement (ii) contradicts the conclusions of [2, 13-14] obtained from classical principles of [4]. In our opinion, the one-electron approximation for calculating the interaction energy of the valence shell of noble element atoms with the electromagnetic field can be valid only for OFI of the first electron, since its first excited state is sufficiently high. The interaction energy of other electrons of the valence shell with the electromagnetic field cannot be taken into account within the classical one-electron approximation and requires inclusion of a rather dense spectrum of strongly correlated states.

IV. PRELIMINARY EXPERIMENTS ON OBSERVATIONS OF THE X-RAY LASER WITH λ = 32.8 NM IN THE KRYPTON CLUSTER JET

The first experiment on observations of the XRL in Kr^{8+} caused by interaction of the krypton cluster jet with a pump laser was performed in [15], where a Ti-sapphire laser system (10 TW, 45 fs, 235 mJ, 810 nm, 10 Hz) was used. The beam was focused into a spot of diameter $d = 10$ μm which corresponded to an intensity of $4 \cdot 10^{18}$ W/cm^2. The pump pulse was circularly polarized; the polarization ellipticity was varied using a $\lambda/4$-motorized plate. The cluster jet was formed in a slit valve; the target/plasma length was 9 mm. The pump pulse was directed along the slit. The experiment was performed in two main approaches: (i) plasma generation using one of the above-mentioned pump pulses and (ii) in addition to the pump pulse, in 2.5 ns, plasma was irradiated with an "ignition pulse" (45 fs, p-polarized, 45 mJ) and, in 80 ps, by a "plasma heating pulse" (45 fs, s-polarized, 300 mJ). The last two pulses formed a so-called waveguide, i.e., quasi-homogeneous plasma in the active state, which provides XRL pulse propagation with a small divergence angle. All pump beams passed through an axicon.

Without the above-described "waveguide", the maximum quantum yield $N_{out}^{ph} = 1.5 \cdot 10^8$ photon/pulse at $n_{Kr} = 6 \cdot 10^{17}$ at/cm^3; the XRL output beam divergence was 15 mrad. When using the waveguide, $N_{out}^{ph} = 8 \cdot 10^{10}$ photon/pulse at $n_{Kr} = 1.6 \cdot 10^{19}$ cm^{-3}; it corresponded to the conversion efficiency of $2 \cdot 10^{-6}$; the divergence was 5.6 mrad. Figure 3 in [15] shows that a high XRL yield is also possible at $n_{Kr} > 2 \cdot 10^{19}$ cm^{-3} at T_e achieved in [15]. In that experiment, plasma contained Kr^{9+} and Kr^{10+} ions after the first pump pulse with a too high intensity. Then, plasma recombined for 2.5 ns, extended and cooled due to the radiation and recombination loss, reaching the Kr^{8+} stage; in

this case, plasma in the active region became more homogeneous. Without the use of secondary (heating) pulses, amplification occurred in the cooling mode at low T_e. The corresponding dependence of N_{out}^{ph} on n_{Kr} is shown by open circles in Fig. 3 in [15]. When using secondary pump pulses, plasma recombining to the state where ground-state Kr^{8+} ions dominated, was heated again due to inverse bremsstrahlung absorption of photons. It is clear that T_e in the latter case was significantly higher; in this case, the optimum value of n_{Kr} increased to ~$2 \cdot 10^{19}$ cm^{-3}; the corresponding dependence of N_{out}^{ph} on n_{Kr} is shown by solid circles in Fig. 3 in [15].

In the following study [16], the experimental method for XRL observation in krypton cluster plasma was improved by using the 25th harmonic of the Ti-sapphire laser, generated in argon gas. Passing through the active medium, the high harmonic (HH) is also amplified. When using the high harmonic with the same wavelength as the XRL, the superposition of two waves having an effect on each other is in fact amplified. One of them (HH) has a high degree of coherence and ultrashort duration. The effect of the HH on the XRL line is strong enough. This results in a decrease in the lasing duration, a decrease in the amplified radiation divergence, and an increase in its coherence.

The XRL output radiation coherence was measured in [16] by a two-slit Young interferometer. It was found that the spatial coherence of the XRL using the high harmonic increases by a factor of ~4 in comparison with the same XRL without HH. In [16], $N_{out}^{ph} = 10^{11}$ photon/pulse, the XRL beam divergence at half maximum was 1.1 mrad. In the recent work [1], the same scheme as in [15-16] was used; however, the main pump pulse in [1] was ~1 J. In [1], it was found that the pump intensity of $2 \cdot 10^{17}$ W/cm^2 during the interaction with the jet of krypton clusters ~500Å in size (>10^4 atom/cluster) provides plasma in which ions in the Kr^{8+} state dominate.

V. MODEL CALCULATION OF THE X-RAY LASER WITH λ = 32.8 NM IN KRYPTON CLUSTER PLASMA

In the experiments with cluster plasma [1, 15-16], the principal problem was solved, i.e., the achievement of the high degree of coherence in relatively long plasma with $L \sim 1$ cm. In this case, plasma with a temperature of ~10 keV was cooled for a recombination time of 2.5 ns, reaching the active Kr^{8+} ion state. Thus, almost the entire deposited energy was emitted for the recombination time. Our principal idea is that the high conversion efficiency and the high degree of coherence can be achieved in an extremely small plasma volume $V \sim 10^{-8}$ cm^3 due to the use of extremely high T_e and n_{Kr}. Let us present the basic prerequisites for developing highly efficient XRLs in cluster jets.

(i) More than 90% absorption of the pump energy is possible; this was shown, e.g., in the experiment [17] for noble gas cluster jets at the plasma pumping peak intensity of ~10^{17} W/cm^2. (ii) Weak reflection of the pump beam from the cluster jet and the absence of fragments in plasma. (iii) An electron energy of several keV can be achieved. For example, in [18], the distribution of electrons with energies of several keV due to the xenon cluster jet irradiation with an intense laser beam was recorded. In other early experiments [19], it was found that high electron temperatures are achieved during irradiation of rather large clusters: at the cluster diameter of 150 Å, T_e>1 keV is achieved at an intensity of ~10^{16} W/cm^2; as the intensity is increased to $5 \cdot 10^{16}$ W/cm^2, $T_e \sim 10$ keV (see Fig. 9 in [19]). (iv) The plasma density and temperature as well as the ionization balance can be controlled. (v) In the cluster jet with high velocity, the XRL pulse repetition with ~125 kHz [20] is possible.

A large number of parameters characterizing (i) plasma and its configuration, (ii) the nozzle, pressure in a gas container, and cluster size, and (iii) the laser pump pulse should be made consistent using a theoretical model. Then the active medium can in principle be produced by one main pump pulse. This is possible if the model adequately reproduces experimental data.

The cluster size is of crucial importance for high-temperature plasma formation during the interaction of the ultrashort pump pulse with the cluster jet. The pulse pedestal is usually several nanoseconds; during the interaction of the pulse pedestal with the cluster, the latter is heated, electrons emit from atoms and the cluster surface, and the cluster expands. The highest value of T_e is achieved, when n_e in cluster nanoplasma is $3 \cdot n_{crit}$ ($n_{crit} = \pi c^2 me/e^2 \lambda^2$): the laser frequency is equal to the plasma frequency; in this case, the resonant contribution of the laser energy to the

plasma energy occurs [19]. To achieve the maximum energy deposition, the pedestal duration and intensity should correlate with the cluster size: if the cluster is too small (rapidly expands reaching $3 \cdot n_{crit}$), the cluster explodes too rapidly (before arrival of the main intense pulse), plasma T_e is low. If the cluster is too large (expands for a too long time), the cluster explodes after the intense pulse passage, plasma T_e is also low. The regular-size cluster reaches $n_e = 3 \cdot n_{crit}$ at the instant of the arrival of the main femtosecond pump pulse; in this case, plasma T_e has a maximum possible value.

The cluster sizes depending on the gas pressure and temperature in the initial back camera, and the valve configuration are well studied for conical valves with round orifice, for which the number of atoms in noble gas clusters is usually determined by the Rayleigh scattering method using an empirical formula [21]. Recently, cluster sizes for the slit nozzle began to be studied depending on the gas pressure in the initial chamber. For example, in [22], it was shown that the slit supersonic nozzle provides a significantly larger number of atoms in the cluster in comparison with the conical nozzle.

The dependences of the plasma electron and ion energies on the cluster size were studied in many experiments, e.g., in [18, 23]. In [18], the xenon cluster jet was irradiated with a laser with a peak intensity of 10^{16} W/cm^2; it was shown that xenon atom clustering begins as the pressure in the initial chamber is increased to a pressure of ~1 bar. The cluster size increases with increasing pressure, which leads to a rapid increase in the plasma electron temperature (see Fig. 2 in [18]). The T_e growth curve with increasing density is qualitatively identical to our result obtained in [7] and showed there in Fig. 4. To continue this curve to the region of very high plasma density ($n_i \geq 10^{18}$ cm^{-3}, which corresponds to the cluster size of $\geq 10^3$ atom/cluster), we use Fig. 4 of [23]. The resulting dependence of T_e on n_i is shown in Fig. 6. The inset in Fig. 6 shows the corresponding dependence of T_e on the cluster size for Xe and Kr. We will use this dependence in the gain $g(t)$ calculations. As seen in Fig. 6, T_e for Kr clusters decreases at larger cluster sizes (larger n_{Kr}). This means that a more efficient XRL can be developed in the region of high densities in Kr^{8+} than in Xe^{8+}.

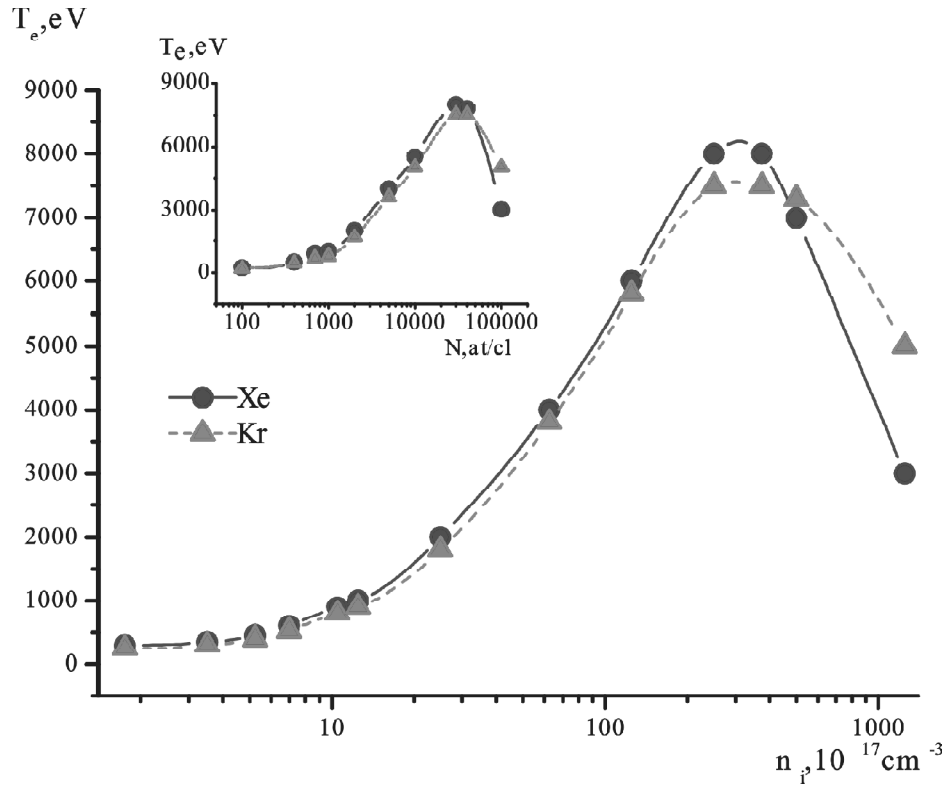

Figure 6: Dependence of the plasma electron temperatures T_e on the density n_{Kr}, n_{Xe} The result is obtained using our calculations [7] and experimental and theoretical data of [23]. The inset shows the dependence of the plasma electron temperature on the number of cluster atoms N.

The XRL calculation model was used in our previous works [6-8] in which references to the detailed description of the theoretical approach are given. The theoretical approach is briefly described in section 2. When using a cluster jet as a target, plasma heating results from an explosion of a weakly ionized expanded cluster; at the initial time after explosion, $T_i >> T_e$; however, electron-ion temperatures at high plasma densities ($(n_i \geq 10^{19}$ cm^{-3}) are thermalzed in the time interval of ≤100 fs. Therefore, in the present calculation, we use $T_e = T_i$; this condition has a significant effect on the Doppler contribution to the laser transition linewidth; nevertheless, at high densities ($n_i \geq 10^{19}$ cm^{-3}), the line broadening caused by electron-ion collisions exceeds the Doppler broadening.

Let us determine the plasma optimum conditions using the dependence of T_e and T_i on the atomic density n_{Kr}, shown in Fig. 6. The time evolution *g(t)* for one of the optimum values $n_{Kr} = 8.75 \cdot 10^{19}$ cm^{-3}, $T_e = 5800$ eV, $d = 12$ μm is shown in Fig. 5. The value of *g(t)* at the maximum is above 1000 cm^{-1}. Averaging over the interval of 1 ps, $G_{av} \approx$ 800 cm^{-1}. For comparison, Fig. 5 shows *g(t)* and G_{av} for the XRL formed by OFI of gaseous krypton [13], where averaging is performed in the interval of ~20 ps. Figure 5 also shows the evolution *g(t)* in cluster plasma [15] which, after cooling, was heated using secondary pump pulses; in this case, averaging was performed in the interval of ~10 ps. We note that 10 ps correspond to the spatial scale of XRL pulse damping of about 3 mm. Propagation of the spatial pulse of such a scale was observed in [24], where experimental conditions were identical [15].

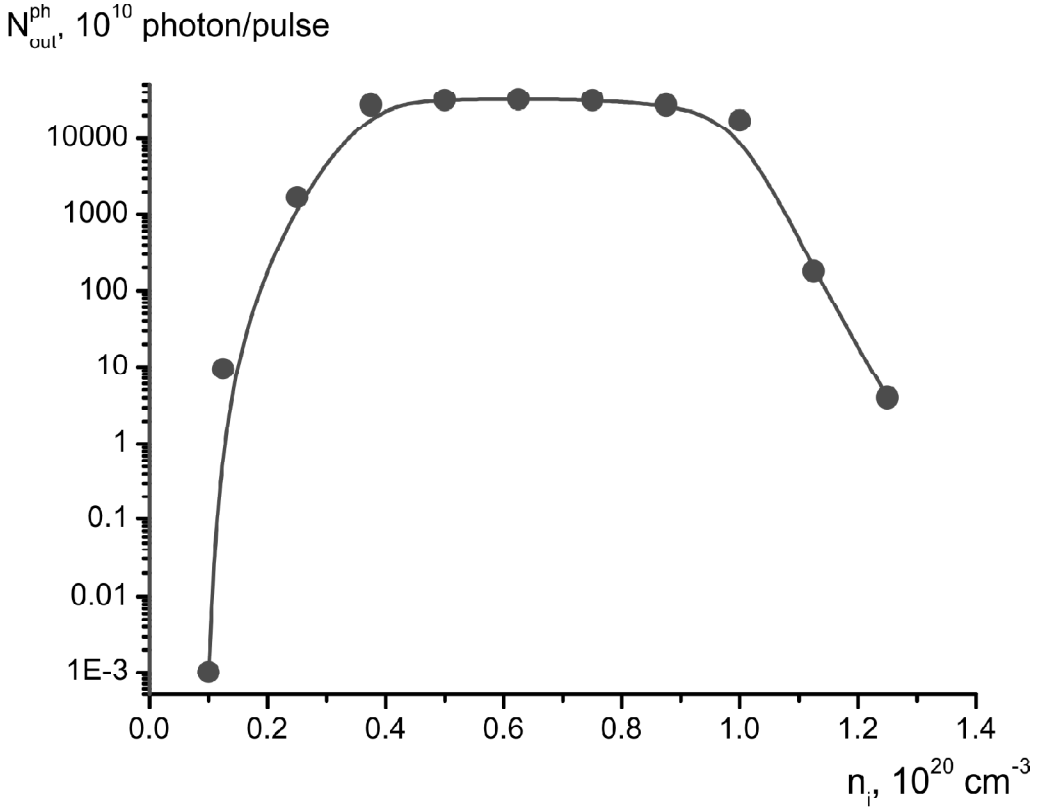

Figure 7: Quantum yield of the model calculation for the XRL at a wavelength of 32.8 nm with a pulse duration of ~1 ps from a volume of ~10^{-8} cm^3 as a function of the Kr^{8+} ion density at T_e = 5800 eV.

Let us calculate the quantum yield per 1 ps for a cylinder with $L = 300$ μm, $d = 12$ μm with volume $V = 3.4 \cdot 10^{-8}$ cm^3, its dependence on the density is shown in Fig. 7. $N_{out}^{ph} > 10^{14}$ for the wide range $n_i \approx (4\text{-}9) \cdot 10^{19}$ cm^3. This corresponds to $n_e \approx (3\text{-}8) \cdot 10^{20}$ cm^3, and the total energy absorbed in the volume V should be ~$(1\text{-}3) \cdot 10^{17}$ eV.

VI. EXPERIMENTAL SETUP

It is known [22] that the slit valve exhibits the strongest pressure dependence of the average cluster size. The supersonic nozzle is more efficient for forming large clusters than the sonic nozzle. We use the slit supersonic

nozzle with a slit width of 500 μm and a slit half-opening angle of 24°. The krypton pressure before the valve is varied within 35-45 atm. The nozzle operates in the pulsed mode. At least two conical diaphragms with slit holes (skimmers) are placed in the path of the cluster jet. The diaphragms form the cluster beam with a given density, whose cross section is a rectangle 300 μm wide and 5 mm long. The cluster beam width defines the plasma column length L. The pump pulse and HH are focused into a cluster jet perpendicular to the jet length. At the above pressures, the gas phase in the cluster jet is almost absent, and the cluster size is represented as a certain distribution.

The optical scheme of the experimental setup for generating the ultrashort XRL pulse in Kr^{8+} ions is shown in Fig. 8. The krypton cluster jet (1) is rectangular-shaped and is directed normally to the plane of Fig. 8, so that focused radiation of the pumping laser beam touches the bottom edge of the rectangular cross section of the krypton cluster jet. This is done to minimize the cluster plasma radiation loss due to radiation absorption in the direction perpendicular to the XRL optical axis (2). To pump plasma and to organize femtosecond shutters, the system based on the Ti-sapphire laser (λ = 810 nm) is used, which generates four independent laser pulses: the main one (3) and three additional pulses (4, 5, 6) delayed with respect to the main pulse. The main laser pulse with an intensity of ~$2 \cdot 10^{17}$ W/cm^2 ionizes krypton clusters, forming plasma in which Kr^{8+} ions dominate. The first additional laser pulse (4) with an energy of ~1 mJ, interacting with gaseous argon, generates the 25th harmonic (HH) which arrives at cluster plasma (1) with a delay of ~100 fs with respect to the main pump pulse (3). HH radiation decreases the XRL beam divergence, reduces the XRL pulse duration, and increases spatial coherence. The second (5) and third (6) additional pulses organize ultrafast plasma shutters used for recording the plasma and XRL radiation parameters.

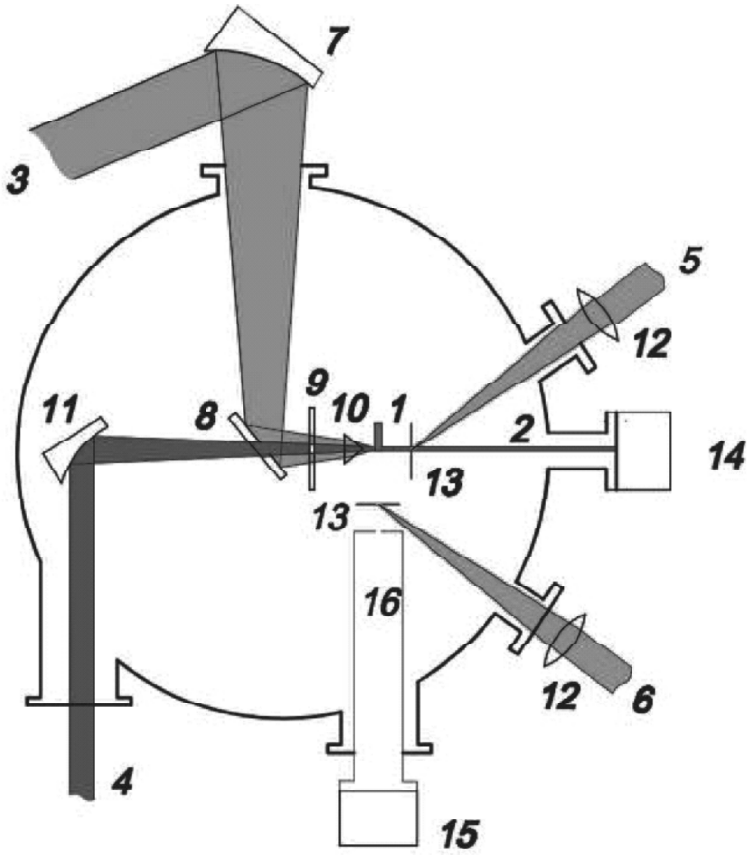

Figure 8: Schematic description of the setup for generating ultrashort XRL pulse: (1) krypton cluster jet cross section, (2) XRL axis, (3) main pump pulse, (4) the first delay line for the HH pulse, (5, 6) the second and third delay lines, i.e., ultrafast optical plasma gates, (7) off-axis parabolic mirror, (8) plane deflecting mirror, (9) polarizer, (10) axicon, (11) multilayer parabolic mirror, (12) lenses, (13) aluminum filters, (14) grazing incidence spectrometer + CCD camera, (15) camera obscura, and (16) high-vacuum region of the measuring channel.

The main laser pulse parameters are 10 mJ, 50 fs; the temporal contrast is $>10^7$ at t~10 ns, $>10^6$ at t~50 ps, and $>10^4$ at t~1 ps. The diameter of the focal spot of laser radiation on the cluster jet surface is 10 μm.

Tuning «chirps» achieve the exact identity of XRL and HH wavelengths during HH generation. The argon cell length is optimized and is 6.5 mm, the argon pressure is ~22 Torr. To focus the main laser pulse into the krypton cluster jet, an off-axis parabolic mirror (7) was used, after which the pulse is reflected from a plane deflecting mirror (8), passes through a polarizer (9) and, using an axicon (10), forms an extended caustic with the Bessel intensity distribution at the cluster jet cross section.

The HH pulse, using a multilayer parabolic mirror (11) (λ = 32.8 nm), is also focused into a krypton cluster jet coaxially with the main pulse, preliminarily having passed the polarizer (9) and through central holes in the mirror (8) and axicon (10). The ellipticity of both pulses is optimized by the polarizer (9).

The HH pulse comes to cluster plasma in ~100 fs after the end of the main pump pulse. Additional pulses (5) and (6) pass through the second and third delay lines, respectively, to form ultrafast shutters absorbing residual radiation in ≤1 ps after the XRL emission start. Pulses (5) and (6) are focused by lenses (12) to aluminum foils (13) 300-400 nm thick, which are commonly used as filters when recording radiation in the range of 30-40 nm. These laser pulses provide ultrafast ionization (explosion) of the outer region of foil filters, converting them into low-temperature plasma absorbing radiation residue (afterglow) from the plasma active region. During the setup adjustment and synchronization, the filter is mechanically replaced before each laser pulse to provide reproducible plasma formation conditions on foils.

To diagnose the XRL plasma and radiation parameters, two channels are used to record the parameters along (14) and across (15) the XRL optical axis. To prevent the XRL spectrum broadening, the second measuring channel (16) is made closest to cluster plasma and is pumped to a pressure of 10^{-8} Torr at the background krypton pressure of 10^{-5} Torr in the vacuum chamber. The high vacuum region is separated from the low vacuum region by an aluminum filter. Diagnostic devices can be installed on flanges of measuring channels in various combinations.

The XRL and HH wavelengths are recorded by a grazing incidence spectrometer equipped with a CCD camera. An interferometric method is developed to measure the line profile which cannot to be resolved using a diffraction spectrometer, since the output XRL and HH pulses will be extremely narrow (~1 mÅ) due to high gains. The absolute radiation energy, hence, the XRL efficiency is measured using an AXUV-100G (IRD Inc.) calibrated photodiode placed along the XRL axis (14). To this end, taking into account the photodiode sensitivity, transmittance of Al filter and the profile of the measured transmittance spectrum, the energy of XRL radiation is calculated. The spatial characteristics of emitting plasma are measured using a camera obscura with recording by a CCD camera. The evolution of the amplifying pulse propagation along the plasma column is recorded in the transverse direction. The spectrum measurement start time using this camera is correlated with the time point of the main pump pulse arrival at the cluster jet. The CCD camera placed along the plasma column axis measures the XRL radiation divergence. It is planned to perform the first experiments without the use of HH and axicon for optimizing the ellipticity and cluster parameters in the jet.

VII. CONCLUSION

The detailed calculation showed that the scheme for Kr^{8+} is most efficient for X-ray lasing by the OFI method among three similar schemes presented in [2] and in Fig. 1. The highly efficient ultrashort XRL formed in the krypton cluster jet is based on the possibility of achieving $T_e \geq 5$ keV at $n_{Kr}^{opt} = (4\text{-}8)\cdot 10^{19}$ cm^{-3}, which is optimal. We note that n_{Xe}^{opt} is much lower for XRL generation in cluster plasma at the transition with λ = 41.8 nm in Xe^{8+} [7], where t_{las} ~ 5 ps and $L \geq 1.5$ mm under optimal conditions. The high efficiency of the XRL in Kr^{8+} is caused by the satisfaction of three essential conditions.

(i) Fast excitation of the upper active level $3d^9 4d\ ^1S_0\ [J=0]$ from the ground state $3d^{10}$.

(ii) Fast ionization of Kr^{8+} to higher ionization stages Kr^{9+} and Kr^{10+} due to electron-ion collisions.

(iii) Large $g(t)$ averaged over the time interval of 1 ps. For comparison, we note that the quantum yield about hundred times higher than in Xe^{8+} [8] can be achieved in the XRL of subpicosecond range in Kr^{8+}. This is because high-temperature krypton plasma with $T_e \geq 5000$ eV allows extension to the region of higher density n_{Kr} (see Fig. 6). Furthermore, the rates of level mixing due to electron-ion collisions in Kr^{8+} (transition to the equilibrium state) are approximately two times slower than in Xe^{8+}. It is also important that the Kr^{8+} ionization rate in the subpicosecond time scale occurs in denser plasma than in Xe^{8+} plasma.

The ionization balance is controlled by the pump laser intensity; for example, the intensity of ~$(1\text{-}2)\cdot10^{17}$ W/cm^2 is sufficient to obtain plasma in which Kr^{8+} ions dominate. Ordinary femtosecond lasers have a prepulse of several nanoseconds; the prepulse duration is correlated with a cluster size to achieve a maximum energy deposition of the main femtosecond pump pulse.

In modern experimental approaches to XRL developments, it is commonly accepted that the amplification drop with increasing plasma density is caused by a too large plasma density gradient along the radius, which caused a too large ionization induced refraction gradient and coherence loss. Our numerous calculations show that this conclusion is only a problem part. The maximum of the dependence of the quantum yield on density is caused by the balance of the processes of increasing inversion and the level population tendency to an equilibrium state, i.e., inversion violation.

The possibility of developing the XRL in Kr^{8+} with a conversion factor of $5\cdot10^{-3}$ of the total pump energy is indirectly confirmed by recent experiments [1, 24], where a relatively high conversion factor ($5\cdot10^{-6}$) of the XRL in Kr^{8+} was achieved in a plasma ~0.9 cm long and $d = 12$ μm with $I_{pump} \sim 4\cdot10^{18}$ W/cm^2 and $n_{Kr} \sim 1.6\cdot10^{19}$ cm^{-3}. At such a high intensity, ions of a higher degree of ionization than Kr^{8+} dominated at the initial time in plasma. At the initial time, T_e was ~10 keV; it is easy to estimate that so dense plasma lost almost entire deposited energy in 2.5 ns after recombination and radiation loss, then plasma was heated again by igniter and heater. In the model under consideration, it is proposed to use the entire deposited energy to XRL radiation due to an increase in the ion density to achieve giant $g(t)$ at a submillimeter plasma pinch length.

Table 1
Comparison of atomic data of the Ni- like krypton, calculated in this work and in [2]

		This work	*Lemoff et al. [2]*
Radiative decay probability of transition: $3d^94p\,^1P_1 - 3d^{10}\,^1S_0$	(s^{-1})	$6.84\cdot10^{10}$	$9.52\cdot10^{10}$
Radiative decay probability of transition: $3d^94d\,^1S_0 - 3d^94p\,^1P_1$	(s^{-1})	$1.64\cdot10^{10}$	$\sim4.00\cdot10^{10}$
Electron energy distribution		Maxwell 100% of electrons: T_e = 640 eV	Non-Maxwell; 100% of electrons: from 12 to 1050 eV,
Ion energy		$T_i=T_e/10$	
Electron induced transitions:	(cm^3/s)		
$3d^{10}\,^1S_0 - 3d^94p\,^1P_1$		$2.7\cdot10^{-9}$	$7.3\cdot10^{-9}$
$3d^{10}\,^1S_0 - 4d^94d\,^1S_0$		$1.3\cdot10^{-8}$	$9.9\cdot10^{-9}$
$3d^94d\,^1S_0 - 3d^94p\,^1P_1$		$1.4\cdot10^{-8}$	$7.9\cdot10^{-8}$
$3d^94d\,^1S_0 - 3d^94f\,^1P_1$		$2.1\cdot10^{-8}$	$1.9\cdot10^{-7}$
Electron collision line width (λ = 32.8 nm) at $n_i = 10^{17}$ см$^{-3}$, $n_e = 8\cdot10^{17}$ см$^{-3}$	(ns^{-1})	128	122
Doppler width	(ns^{-1})	388	115
Inversion calculations		Kinetic equations calculations for 68 levels of Kr^{8+}	$N^*=N_i^2(R_{up}\text{-}1/3R_l)\cdot(1/\tau_{up}+N_iR_{out})$
Maximum inversion density	(cm^{-3})	1.1×10^{15}	1.0×10^{15}
Gain	(cm^{-1})	19	94

It follows from the experiments [15-16] that plasma is formed in the cluster jet immediately after the interactions of the pump pulse with plasma. Emission with $\lambda = 32.8$ nm during cluster expansion is negligible. At high plasma densities, the XRL intensity reaches a maximum in 100 fs (see Fig. 5). Thus, in the XRL project under consideration, the pulse with an extremely sharp front edge of output XRL radiation and the absence of pedestal can be obtained; the XRL pulse is also characterized by a steep edge due to optical gate (5) in Fig. 8. Such a pulse shape seems promising for studying ultrafast processes.

The authors are grateful to G.N. Makarov and S.V. Chekalin for attention to the study and helpful discussions.

References

[1] B.K. Chen, Y.-C. Ho, T.-S. Hung, Y.-L. Chang, M.-C. Chou, S.-Y. Chen, H.-H. Chu, S.-L. Huang, P.-H. Lin, J. Wang, J.-Y. Lin, "High-brightness optical field-ionization collisional-excitation extreme-ultraviolet lasing pumped by 100-TW laser system in an optically preformed plasma wave guide", *Appl. Phys. B* **106**, 817 (2012).

[2] B.E. Lemoff, C.P.J. Barty, and S.E. Harris, "Femtosecond-pulse-driven, electron excited XUV lasers in eight-times-ionized noble gases", *Opt. Let.* **19**, 569 (1994).

[3] L.N. Ivanov, E.P. Ivanova, L.V. Knight, "Radiative transition probabilities for Ne-like ions. Consistent quantum mechanical calculations", *Phys. Lett. A* **206**, 89 (1995).

[4] P.B. Corkum, N.H. Burnett, and F. Brunel, "Above-Threshold Ionization in the Long-Wavelength Limit", *Phys. Rev. Lett.* **62**, 1259 (1989).

[5] J.J. Rocca, D.P. Clark, J.L.A. Chilla, V.N. Slyaptsev, "Energy excitation and achievement of the saturation limit in a discharge-pumped table-top soft x-ray amplifier", *Phys. Rev. Lett.* **77**, 1476 (1996).

[6] E.P. Ivanova, N.A. Zinoviev, "Calculation of the vacuum-UV radiation gains in transitions of the Ne-like argon in capillary discharges", *Quantum Electronics* **29**, 484 (1999).

[7] Ivanova E.P., "High efficient X-ray laser at l=41.8 nm in Pd-like xenon pumped by optical field ionization in a cluster jet" *Phys. Rev. A* **84**, 3829 (2011).

[8] E.P. Ivanova, "Subpicosecond 41.8 nm X-ray laser in the plasma produced by femtosecond laser irradiation of a xenon cluster jet" *Quantum Electronics,* **42**,1100 (2012).

[9] Larroche O., Ros D., Klisnick A., Sureau A., Möller C., Guennou H., "Maxwell-Bloch modeling of x-ray-laser-signal buildup in single- and double-pass configurations", *Phys. Rev. A*, **62**, 043815 (2000).

[10] C.M. Kim, A. Janulewicz, H.T. Kim, and J. Lee, "Amplification of a high-order harmonic pulse in an active medium of a plasma-based x-ray laser", *Phys. Rev. A*, **80**, 053811 (2009).

[11] J. Zhang *et al*, "A saturated X-ray Laser Beam at 7 Nanometers", *Science* **276**, 1097 (1997).

[12] E.P. Ivanova and N.A. Zinoviev, "Time history of gain calculations in radiative-collisional model for X-ray lasers", *J. Phys. IV. France,* **11**, Pr2-151 (2001).

[13] S. Sebban *et al*., "Demonstration of a Ni-like Kr Optical-Field-Ionization Collisional Soft X-Ray Laser at 32.8 nm", *Phys. Rev. Lett.*, **89**, 253901 (2002).

[14] S. Sebban *et al*., "Saturated Amplification of a Collisionally Pumped Optical-Field-Ionization Soft X-ray Laser at 41.8 nm", *Phys. Rev. Lett.,* **86**, 3004 (2001).

[15] M.-C. Chou, P.-H. Lin, C.-A. Lin, J.-Y. Lin, J. Wang, and S.-Y. Chen, "Dramatic Enhancement of Optical-Field-Ionization Collisional-Excitation X-Ray Lasing by an Optically Preformed Plasma Waveguide", *Phys. Rev. Let.*, **99**, 063904 (2007).

[16] P.-H. Lin, M.-C. Chou, M.-J. Jiang, P.C. Tseng, H.-H. Chu, J.-Y. Lin, J. Wang, and S.-Y. Chen, "Seeding of a soft-x-ray laser in a plasma wave guide by high harmonic generation" OPTICS LETTERS, **34**, 3562 (2009).

[17] T. Ditmire, R.A. Smith, R.S. Marjoribanks, G. Kulcsar, and M.H.R. Hutchinson, "X-ray yields from Xe clusters heated by short pulse high intensity lasers", *Appl. Phys. Lett.* **71**,166 (1997).

[18] Y.L. Shao, T. Ditmire, J.W.G., Tisch, E. Springate, J.P. Marangos, and M.H.R. Hutchinson, "Multi-keV Electron Generation in the Interaction of Intense Laser Pulses with Xe Clusters", *Phys. Rev. Lett.,* **77**, 3343 (1996).

[19] T. Ditmire, T. Donelly, A.M. Rubenchik, R.W. Falcone, M.D. Perry, "Interaction of intense laser pulses with atomic clusters" *Phys. Rev. A*, **53**, 3379 (1996).

[20] S. Ter-Avetisyan, U. Vogt, H. Stiel, M. Schnürer, I. Will, and P.V. Nickles, "Efficient extreme ultraviolet emission from xenon-cluster jet targets at high repetition rate laser illumination", *J. Appl. Phys.* **94,** 5489 (2003).

[21] O.F. Hagena and W.J. Obert, "Cluster Formation in Expanding Supersonic Jets: Effect of Pressure, Temperature? Nozzle Size, and Test Gas", *J. Chem Phys.* **56,** 1793 (1972).

[22] G. Chen, B. Kim, B. Ahn, and D.E. Kim., "Pressure dependence of argon cluster size for different nozzle geometries", *J. Appl. Phys.* **106**, 053507 (2009).

[23] E. Springate, N. Hay, J.W.G. Tisch, M.B. Mason, T. Ditmire, M.H.R. Hutchinson, and J.P. Marangos, "Explosion of atomic clusters irradiated by high-intensity laser pulses: Scaling of ion energies with cluster and laser parameters", *Phys. Rev. A.* **61**, 063201 (2000).

[24] M.-C. Chou, P.-H. Lin, T.-S. Hung, J.-Y. Lin, J. Wang, and S.-Y. Chen, "Experimental investigation of the parameter space for optical-field-ionization cluster-jet x-ray lasers" *Phys. Rev. A*, **74**, 023804 (2006).